

Large-scale Molecular Dynamics Simulation of Perfluorosulfonic Acid Membranes: Remapping Coarse-Grained to All-Atomistic Simulations

An-Tsung Kuo^{1†}, Yusuke Miyazaki^{2†}, Changwoon Jang², Tatsuya Miyajima¹,
Shingo Urata¹, Steven O. Nielsen³, Susumu Okazaki², and Wataru Shinoda^{2*}

¹Innovative Technology Laboratories, AGC Inc., Yokohama, Kanagawa 221-8755, Japan

²Department of Materials Chemistry, Nagoya University, Nagoya 464-8603, Japan

³Department of Chemistry and Biochemistry, University of Texas at Dallas, Richardson TX
75080, USA

*Corresponding author. Tel: (+) 81-52-789-5288. Fax: (+) 81-52-789-5118.

Email: w.shinoda@chembio.nagoya-u.ac.jp

†These authors contributed equally to the work.

ABSTRACT

We combined two reverse mapping methods, a predetermined fragment database and fragment rotation, to generate atomistic configurations from coarse-grained structures. The combined method together with molecular dynamics simulations was applied to simulate perfluorosulfonic acid (PFSA) membranes with large length scales and to explore the origin of fracture under a uniaxial tensile loading. Through the analysis of voids in the deformed membrane, we found that void growth with tensile loading takes place at the boundary of the hydrophobic and hydrophilic regions, which may be the origin of the fracture in the PFSA membrane. This study demonstrates an efficient reverse mapping method, which is useful for simulating proton exchange membranes with realistic chain lengths.

KEYWORDS

Proton exchange membrane; Fuel cell; Perfluorosulfonic acid; Molecular dynamics simulation; Coarse grained molecular dynamics simulation; Reverse mapping

The phase-segregated morphology of a hydrated PFSA membrane affects the proton transportation and mechanical characteristics of the membrane. The membrane morphology has thus been extensively studied for achieving efficient proton transport and for designing new materials applicable to PEMFCs [4, 9-16]. Several morphological models, such as the cluster-network model [9, 10], fibrillar structure model [11, 12], parallel-cylinder model [13], and film-like model [14], have been proposed to describe the behavior upon water swelling. Recently, we have used all-atomistic (AA) molecular dynamics (MD) simulations to explore the morphology of hydrated PFSA membranes with molecular weight $\sim 10^4$ [15, 16]. These studies found that the water morphology changes from a channel-network structure to a tortuous layer structure in the shorter side chain PFSA membranes with increasing water content, while the morphology changed to a fat network in the longer side chain PFSA membranes. Since the PFSA models studied by AA-MD simulations differ from the commercially available PFSA polymers especially with respect to the polymer chain length (or molecular weight), larger size MD models are desired for direct quantitative comparison with experiments and for investigations of new PEMFC materials. However, such large-scale AA-MD simulations require inordinate computational resources.

One strategy to reduce the computational cost is to use a coarse-grained (CG) model. Many types of CG simulations, such as dissipative particle dynamics [17-25], self-consistent mean field calculation [26, 27], and CG-MD [22, 28-30], have been applied to investigate the morphology and mechanical properties of PFSA membranes. The CG models can qualitatively describe the properties observed in experiments; however, they are sometimes not accurate enough for quantitative investigation due to the eliminated degrees of freedom (e.g., lack of explicit hydrogen bonding). To address the drawback of CG modeling, a feasible approach is to convert an equilibrated CG system into the corresponding AA model, following a procedure termed reverse mapping or back-mapping. Thus, a combination of CG

simulation with low computational demand and AA-MD simulation at a higher resolution makes it possible to accurately examine the morphology and mechanical properties of PFSA membranes.

In general, the process of reverse mapping consists of two stages: (1) the generation of an AA structure from coarse-grained coordinates and (2) the relaxation of the AA structure [31, 32]. Typically, the published methods for reverse mapping are aimed at either near-optimal AA reconstruction [33-35] or reasonable AA reconstruction requiring only a short AA simulation to relax the structure [32, 36-40]. For example, idealized fragment configurations selected from a predetermined database for reverse mapping CG beads has been applied to generate a near-optimal reconstruction [35]; in the protein folding literature this procedure is called the rotamer library approach [41]. Rotating the fragments for optimal alignment with neighboring fragments has been used to shorten the relaxation time [36, 38].

In this study, we combined the above two reverse mapping methods for generating AA initial structures from coarse-grained coordinates. The combined method was adopted to explore the origin of the fracture in large-scale PFSA membranes with realistic polymer chain length under a uniaxial tensile loading. It should be noted that in the CG model, the system response to applied stress is flawed because of the eliminated degrees of freedom which limit the energy dissipation pathways. In this sense we need to use an AA force field to study the mechanical behavior under applied stress. Thus, after generating a reasonable structure of the polymer membrane in an efficient manner with the CG model, a reliable reverse-mapping method is needed to generate a well-prepared AA configuration.

This paper has been arranged into four Sections. In Section 2, the details of the simulation methods including AA-MD, CG-MD and the combined reverse mapping are described. Section 3 presents the simulation results on validation of the reverse mapping method, and discusses the origin of fracture in PFSA membranes under the uniaxial

deformation. Finally, we summarize the work with several concluding remarks in Section 4.

2. COMPUTATIONAL METHODS

2.1. Coarse-grained model and simulation

In this study, we examined four different chain lengths of PFSA polymer ($x = 4, y = 1, m = 1, n = 2$, see Fig. 1a) with an equivalent weight (EW) of 844. Specifically, the chain lengths consist of 10, 20, 60, and 125 repeat units (termed as 10-, 20-, 60-, and 125-mer hereafter). The 10-mer and 125-mer PFSA polymers were respectively used to validate the combined reverse mapping method and to explore the origin of fracture under the uniaxial tensile loading. The others were used to confirm the equilibrated structure of the 125-mer membrane. The sulfonic acid groups ($-\text{SO}_3\text{H}$) in the pendant side chains were assumed to be fully ionized to H^+ and SO_3^- at all hydration levels (λ), where λ denotes the number of water molecules per SO_3^- ($\lambda = (\text{H}_2\text{O}, \text{H}_3\text{O}^+)/\text{SO}_3^-$). The resulting protons were combined with water molecules to form hydronium ions (H_3O^+).

The hybrid SDK/IBI model [30] was used for the CG-MD simulations of the hydrated PFSA membranes. The CG model of PFSA polymer includes eight types of CG beads as shown in Fig. 1(b). The compatible SDK-CG water model [42], in which three water molecules are packed into a single CG site (denoted as ‘W’), was adopted for the solvent. To represent the hydronium ion, one hydronium ion together with two water molecules is regarded as a single CG site (denoted as ‘H3O’). The details of the hybrid SDK/IBI model can be found in our previous study [30].

In order to construct initial configurations for the CG-MD simulations, we first built an AA PFSA polymer chain using Discovery Studio 2016 [43]. The AA configuration of the PFSA chain was then mapped to a CG configuration by using the “CG-it” tool, which is a

plugin of Visual Molecular Dynamics (VMD) provided by MacDermaid [44]. After that, PACKMOL [45] was used to generate initial CG configurations with low density ($< 0.1 \text{ g/cm}^3$) by arranging CG PFSA chains together with the required water and hydronium CG beads in a cubic box. The water content is controlled at either $\lambda = 3$ or 9. The composition of the simulation systems are listed in Table S1. We note that the initial configurations with low density are used to avoid artificial structures and have been demonstrated to have no influence on the simulation results [15].

The CG simulations in this study were carried out using the LAMMPS MD package [46]. The simulations were first conducted in the microcanonical ensemble (NVE: constant number of atoms, volume and energy) for 1 ns followed by an isothermal-isobaric ensemble (NPT: constant number of atoms, pressure and temperature) MD run for 5 ns at $T = 300 \text{ K}$ and $P = 1 \text{ atm}$. Then, a constant volume MD run of 1 ns was carried out, during which the temperature was increased to 800 K and decreased to 300 K every 250 ps, followed by an NPT run of 5 ns at $T = 300 \text{ K}$ and $P = 1 \text{ atm}$ [15]. The process was repeated four times to confirm that the density had attained a constant value. After that, an equilibration CG-MD run in the NPT ensemble was carried out for 500 ns at $T = 300 \text{ K}$ and $P = 1 \text{ atm}$. When needed, a Nosé-Hoover thermostat [47] and a Parrinello-Rahman barostat [48, 49] with a response time of 0.5 and 5 ps, respectively, were used to control the temperature and pressure. The nonbonded interactions were truncated at 1.5 nm, while the Coulomb interaction was computed using the particle-particle particle-mesh method [50]. A time step of 10 fs was used for the CG simulations. During the equilibration run, the radius of gyration of the polymer was analyzed to confirm the system achieving equilibrium as shown in Fig. S1 of Supporting Information. After the CG membranes reached equilibrium, the densities were 1.91 and 1.79 g/cm^3 for $\lambda = 3$ and 9, respectively, which are consistent with experimental densities [51].

2.2. Reverse mapping and atomistic simulation

Once well-equilibrated CG membrane systems were obtained, the reverse mapping method was applied to reconstruct the corresponding AA models. In order to require only a short relaxation time after back-mapping, we combined two reverse mapping approaches; the predetermined fragment database approach [35] and the fragment rotation approach [36, 38]. First, for the fragments corresponding to the CG bead types of the PFSA polymer, we extracted a number of AA fragments from an equilibrated structure of a small hydrated PFSA membrane composed of 25 10-mer PFSA chains reported in our previous study. The fragment configurations were extracted from the final snapshot and stored in a database. The database thus contained 25-250 structures for each CG bead type (Fig. 2). For back-mapping the CG W bead, we prepared a single configuration composed of three water molecules which were arranged in a sphere with diameter 4.3 Å. A similar configuration was prepared for the CG H3O bead.

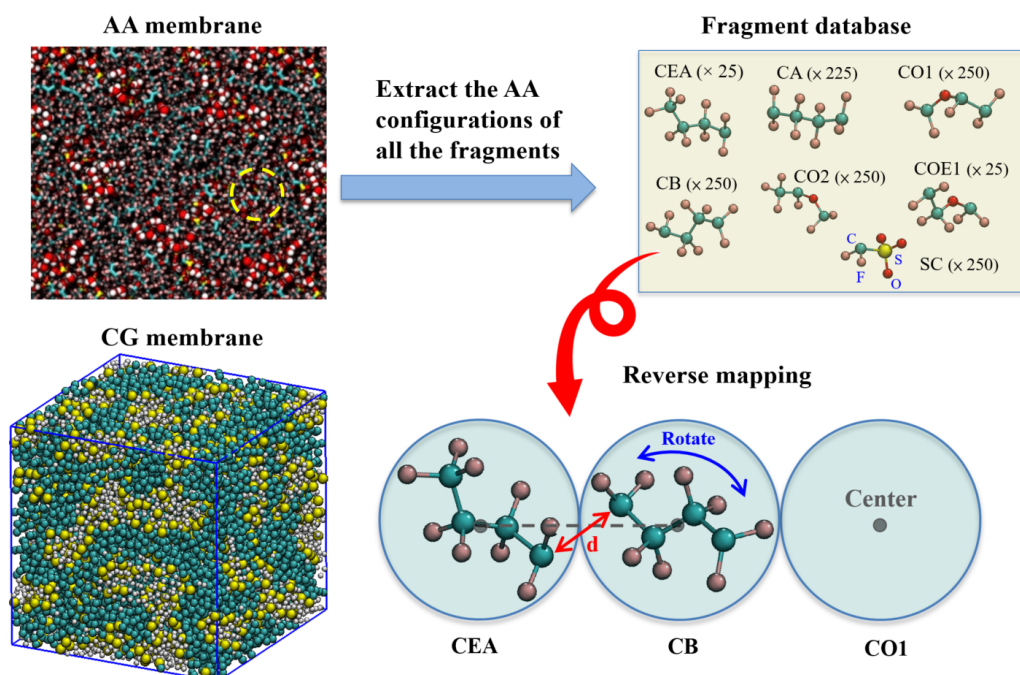


Figure 2. Schematic diagram of the reverse mapping method: (upper panel) assemble the

fragment database and (lower panel) map and rotate one of the fragments in the database.

Then we attempted to map the fragment configurations onto the corresponding CG beads in the equilibrated CG membranes. The mapping procedure was applied sequentially from the head to the end of the CG PFSA chain. As shown in Fig. 2, we randomly chose a fragment from the database and put its center of mass at the corresponding CG bead location. Subsequently, the fragment was rotated using an optimization algorithm over the special orthogonal Lie group $SO(3)$ [38] to satisfy the criterion that the distance between connecting atoms of the neighboring fragments is in the range of $0.9 - 2.1 \text{ \AA}$. If the rotated fragment could not satisfy the distant criterion, the fragment was replaced by another fragment from the database. Sometimes, a couple of neighboring fragments were replaced simultaneously in order to satisfy the distant criterion for all connecting atoms. For the CG beads of W and H3O, we directly put the centers of the predefined configurations mentioned above at the corresponding CG coordinates without rotation.

After generating reasonable atomistic coordinates from the reverse mapping procedure, AA energy minimization was conducted to eliminate overlapped atoms and repair the intramolecular connections at the (AA) link between the neighboring fragments. This is necessary because although the $SO(3)$ optimization algorithm takes account of the AA bond between atoms belonging to adjacent CG beads, it does not consider the AA angle and dihedral potentials involving these bonded atoms nor the van der Waals potential energy terms for the atoms belonging to adjacent CG beads. While it is possible to consider all of these contributions in the $SO(3)$ optimization algorithm, in practice the calculations become overdetermined. For the energy minimization procedure, we first reduced the nonbonded interactions 200-fold so as to avoid excessive forces and used a short steepest descent run. Next, the second step of energy minimization was carried out using a 10-fold reduction of the

nonbonded forces. Finally, we restored the nonbonded forces to their original strength and performed energy minimization to obtain an optimal geometry from which to initiate AA-MD simulations.

Since the W and H3O CG-beads were directly replaced by three molecules, an additional relaxation time was required to redistribute and equilibrate the water molecules. For this purpose we conducted an NVT-MD run of 0.1 ns for the system with unit cell length 12.3 nm and 1 ns for the larger systems. After that, an NPT-MD run of 20 ns was carried out to relax the AA system.

The AA-MD simulations were performed using the Gromacs package, version 5.04 [52, 53]. The modified DREIDING force field by Mabuchi and Tokumasu [54] was adopted for the PFSA polymer. The F3C water model [55] and the classical hydronium model [56] was applied for water molecules and hydronium ions, respectively. Lennard–Jones (LJ) pair interactions were used within a cutoff distance of 1.5 nm without any truncation shift function, and long-range electrostatic interactions were calculated using the particle-mesh Ewald method [57]. The temperature and pressure of the system were controlled using a Nosé-Hoover thermostat [47] and an Parrinello-Rahman barostat [48, 49], respectively. A time step of 1 fs was used to integrate the equations of motion in the AA-MD simulations.

3. RESULTS AND DISCUSSION

3.1. Validation of reverse mapping

In this study, we conducted CG-MD simulations to efficiently equilibrate the large PFSA membrane systems. The reverse mapping procedure was then applied to reconstruct the AA configurations and short AA-MD simulations were performed to equilibrate the AA configurations. Subsequently, the origin of the fracture in the large-scale PFSA membrane models were explored. To validate this strategy, we applied the procedure to the 10-mer

PFSA membrane composed of 200 polymer chains at $\lambda = 9$. The microstructure was compared with that obtained from a single AA-MD simulation without using CG-MD or reverse mapping. The latter model was reported in our previous work [15], where at least 100 ns was required for equilibration [15]. Here we performed an additional 300 ns run to obtain reference data for the comparison.

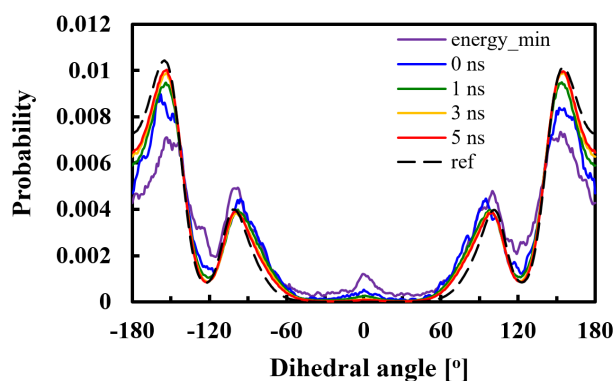


Figure 3. Distribution of C-C-C-C dihedral angle for the reverse mapping PFSA membrane calculated from various AA-MD simulation times post-mapping. “energy_min” and “0 ns” denotes energy minimization and an NVT-MD run of 0.1 ns, respectively. “ref” denotes the AA membrane equilibrated for 300 ns without using reverse mapping.

Since PFSA polymer has a rigid PTFE backbone, it is difficult to obtain a relaxed (equilibrated) configuration of the PFSA membrane within a reasonable AA-MD simulation time without an artificial annealing process, in which cyclic heating and cooling simulations are performed [15]. Contrarily, we did not need to perform the annealing procedure for the AA-MD simulation of the AA model obtained by the reverse mapping method. To confirm this, we first monitored the distribution of C-C-C-C dihedral angles in the reverse mapped membrane at different AA-MD simulation times post-mapping. The result is shown in Fig. 3. It is found that the backbone dihedral angle distribution quickly achieved equilibrium after only 3 ns of relaxation; this is impossible for an ordinary AA-MD simulation equilibrated for

100 ns without an artificial annealing process (Fig. S2). The reason may be ascribed to the following facts: 1) the hybrid SDK/IBI model is a sufficiently accurate CG model for the PFSA membrane [30]; 2) the selected fragment in the reverse mapping procedure provides a suitable configuration for each CG bead; 3) the rotated fragment allows a reasonable polymer chain connection.

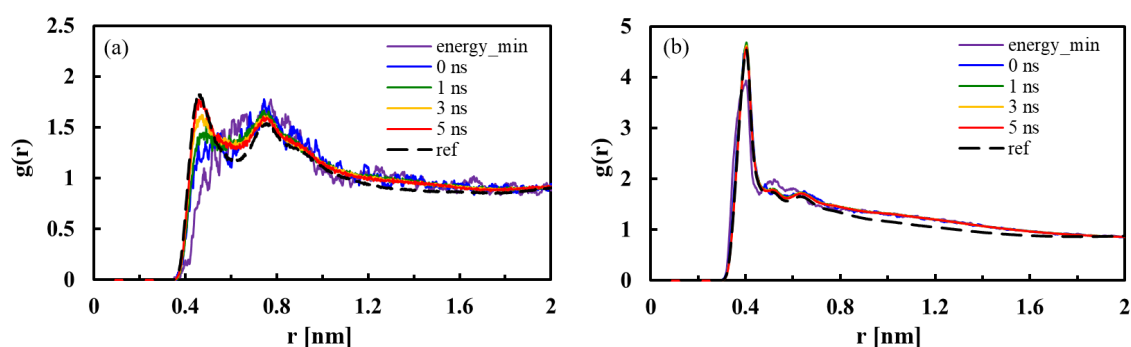


Figure 4. Radial distribution function of (a) sulfur-sulfur (S-S) and (b) sulfur and water oxygen (S-O_w) for the reverse mapping PFSA membrane calculated from various AA-MD simulation times post-mapping. “energy_min” and “0 ns” denotes energy minimization and an NVT-MD run of 0.1 ns, respectively. “ref” denotes the membrane equilibrated for 300 ns without applying reverse mapping.

In addition to the polymer structure, the morphology of the phase separation between the polymer and water regions should need a certain relaxation time, because water molecules were remapped from the CG W and H₃O beads without regard for hydrogen bonding. In particular, the water distribution could affect the PFSA side chain conformations. Hence, we monitored the time variation of the radial distribution function (RDF) of S-S (S: sulfur) and S-O_w (O_w: water oxygen) (Fig. 4). The S-O_w RDF quickly achieved convergence during an NVT-MD run of 0.1 ns (Fig. 4b) due to the high mobility of water around the terminal sulfonic groups. For the S-S RDF (Fig. 4a), the height of the first peak gradually increases

with increasing simulation time up to 5 ns. No significant further change in the RDF could be detected after 5 ns (data not shown). This observation indicates that a 5 ns simulation run is enough for equilibrating the reverse mapped PFSA membrane. These results clearly demonstrate that the reverse mapping approach together with CG-MD simulations can significantly accelerate the equilibration of an atomistic model and consequently lower the required computational resources.

3.2. The origin of fracture in PFSA membranes

The reverse mapping procedure together with CG-MD was applied to explore the origin of the fracture in large-scale PFSA membranes with realistic polymer chain length up to 125-mer using AA-MD simulations. The large-scale simulation system with long polymer chain length usually requires a long computational time. In this study, an NPT-MD run of 20 ns was performed to relax the AA system after the reverse mapping. One may concern whether such short MD run is also sufficient for relaxing the large-scale system with realistic chain length or not. Therefore, an examination of equilibration for the large-scale PFSA membrane is also required before the membrane deformation. Since the independent effect of polymer chain length on the structure and water dynamics of modeled PFSA system has been reported [58], we compared the structural properties of 125-mer PFSA membrane with those of shorter PFSA (i.e. 20- and 60-mer PFSA) membranes to confirm the equilibration of the membranes. The details are shown in Supporting Information.

After obtaining an equilibrated membrane, a uniaxial tensile loading along the z -axis was applied with a constant strain rate of 0.1 ns^{-1} to explore the origin of the fracture for hydrated PFSA membranes. Figure 5 shows the snapshot of the 125-mer PFSA membrane composed of 400 PFSA chains at $\lambda = 3$ at strain = 1.0. One can clearly find that the fracture takes place in the red marked region. Since the fracture of a polymer is related to void

formation and coalescence during tensile loading, we further analyzed the void distribution over the polymer membranes to understand the origin of the fracture. To do so, the simulation systems were divided into small cubic cells with a length of 0.56 nm. Then, the small cells were classified as hydrophobic, hydrophilic, and void cells by counting the atoms in each cell; namely, the cell is categorized as a void cell if it is vacant, otherwise it is judged as hydrophobic or hydrophilic by the ratio of the number of hydrophobic backbone atom to the number of hydrophilic side chain atoms and water. Figure 6 shows snapshots of voids in the 125-mer PFSA membrane with $\lambda = 3$ during the uniaxial tensile loading. No obvious voids are found before the tensile loading. However, some voids are formed and increase in size during the deformation. The regions of significant void growth should be the origin of the fracture in the membrane as shown in Fig. 5.

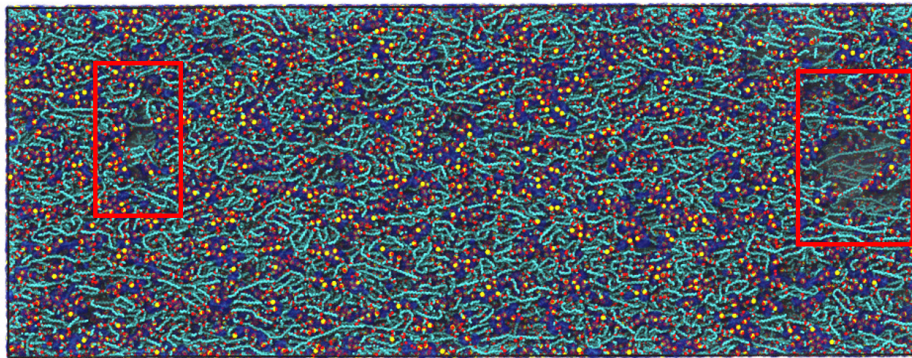


Figure 5. Snapshots of the 125-mer PFSA membrane composed of 400 PFSA chains at $\lambda = 3$ at strain = 1.0. The fracture takes place in the red marked region.

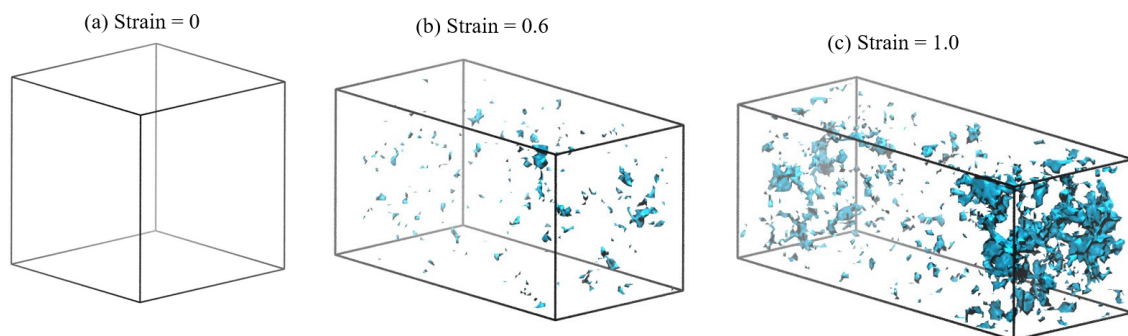


Figure 6. Snapshots of voids in the 125-mer PFSA membrane composed of 400 PFSA chains

at $\lambda = 3$ during the uniaxial tensile loading. The strains are (a) 0, (b) 0.6, and (c) 1.0.

To unravel the occurrence of fracture in the hydrophobic or hydrophilic regions of the membrane, we analyzed the probability of the occurrence of void cells adjacent to each type of cell in the membrane as shown in Fig. 7. The number of contacts can vary from $n = 0$ (no contacts) to $n = 6$ (completely surrounded by that cell type). Before tensile loading at strain = 0, we do observe several void cells in the membrane, although they are not seen in Fig. 6 due to their small number, and from Fig. 7 they are located in the hydrophobic membrane regions. During the deformation, the void cell distributions adjacent to the hydrophobic and hydrophilic cells shift left and right, respectively. This indicates the increasing presence of voids in the hydrophilic/hydrophobic interface region. These results clearly demonstrate that significant void growth occurs at the boundary of the hydrophobic and hydrophilic regions, which may be the origin of fracture in the PFSA membrane.

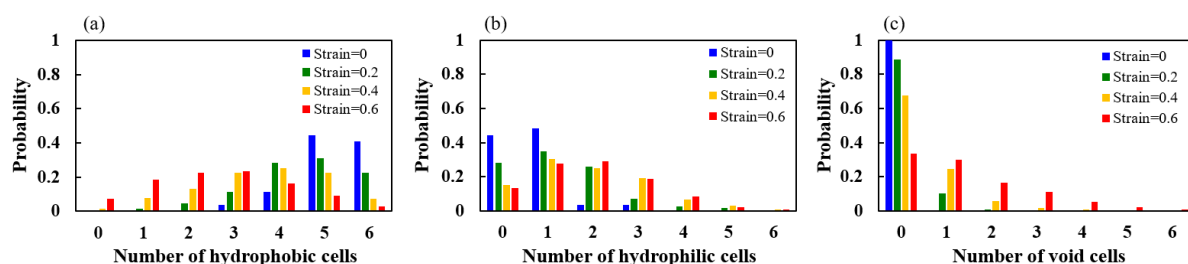


Figure 7. Probability of a void cell adjacent to $n=0-6$ (a) hydrophobic cells, (b) hydrophilic cells, or (c) void cells for the 125-mer PFSA membrane composed of 400 PFSA chains at $\lambda = 3$.

4. CONCLUSIONS

In this work we combined two reverse mapping methods, the predetermined fragment database approach (known in the protein folding literature as the rotamer library approach)

and a rotational optimization algorithm to align the fragments to satisfy the polymer backbone topology, for generating atomistic configurations from coarse-grained structures. The combined method successfully generated a reasonable atomistic reconstruction which only requires a short relaxation time to equilibrate; we found that 5 ns of equilibration was sufficient even though the polymer backbone is very stiff. We applied this combined reverse mapping method together with coarse grained MD simulation to simulate hydrated PFSA membranes with large unit cell sizes and to explore the origin of fracture under a uniaxial tensile loading. Through the analysis of voids in the deformed membrane, we found that the void growth takes place on the boundary of hydrophobic and hydrophilic region, which may be the origin of the fracture. This study demonstrates an efficient reverse mapping method for simulating hydrated PFSA polymer membranes with realistic polymer chain lengths and large length scales, providing insight into the fracture mechanism of the proton exchange membrane.

5. ACKNOWLEDGMENTS

This research was supported by the Impulsing Paradigm Change through Disruptive Technologies (ImPACT) program and by MEXT as a social and scientific priority issue (“Development of New Fundamental Technologies for High-efficiency Energy Creation, Conversion/Storage, and Use”) to be tackled using the post-K computer. Calculations were performed on the facilities of the supercomputer center at Nagoya University; Research Center for Computational Science, Okazaki; the Institute for Solid State Physics, the University of Tokyo; and in part on the K-computer hosted at the RIKEN Advanced Institute for Computational Science (Proposal No. hp150249, hp150275, hp160247 and hp170354).

6. REFERENCES

- [1] C. Iojoiu, F. Chabert, M. Maréchal, N.E. Kissi, J. Guindet, J.Y. Sanchez, From polymer chemistry to membrane elaboration: A global approach of fuel cell polymeric electrolytes, *J. Power Sources* 153 (2006) 198-209.
- [2] Y. Wang, K.S. Chen, J. Mishler, S.C. Cho, X.C. Adroher, A review of polymer electrolyte membrane fuel cells: Technology, applications, and needs on fundamental research, *Appl. Energy* 88 (2011) 981-1007.
- [3] A. Kraytsberg, Y. Ein-Eli, Review of Advanced Materials for Proton Exchange Membrane Fuel Cells, *Energy Fuels* 28 (2014) 7303-7330.
- [4] M. Eikerling, A. Kulikovskiy, Polymer Electrolyte Fuel Cells: Physical Principles of Materials and Operation, CRC Press, Boca Raton, FL, 2014.
- [5] K.A. Mauritz, R.B. Moore, State of Understanding of Nafion, *Chem. Rev.* 104 (2004) 4535-4586.
- [6] M.B. Satterfield, P.W. Majsztrik, H. Ota, J.B. Benziger, A.B. Bocarsly, Mechanical properties of Nafion and titania/Nafion composite membranes for polymer electrolyte membrane fuel cells, *J. Polym. Sci. B* 44 (2006) 2327-2345.
- [7] Y. Tang, A. Kusoglu, A.M. Karlsson, M.H. Santare, S. Cleghorn, W.B. Johnson, Mechanical properties of a reinforced composite polymer electrolyte membrane and its simulated performance in PEM fuel cells, *J. Power Sources* 175 (2008) 817-825.
- [8] A. Kusoglu, A.Z. Weber, New Insights into Perfluorinated Sulfonic-Acid Ionomers, *Chem. Rev.* 117 (2017) 987-1104.
- [9] W.Y. Hsu, T.D. Gierke, Elastic Theory for Ionic Clustering in Perfluorinated Ionomers, *Macromolecules* 15 (1982) 101-105.
- [10] W.Y. Hsu, T.D. Gierke, Ion Transport and Clustering in Nafion Perfluorinated

Membranes, *J. Membr. Sci.* 13 (1983) 307-326.

[11] L. Rubatat, A.L. Rollet, G. Gebel, O. Diat, Evidence of Elongated Polymeric Aggregates in Nafion, *Macromolecules* 35 (2002) 4050-4055.

[12] L. Rubatat, G. Gebel, O. Diat, Fibrillar Structure of Nafion: Matching Fourier and Real Space Studies of Corresponding Films and Solutions, *Macromolecules* 37 (2004) 7772-7783.

[13] K. Schmidt-Rohr, Q. Chen, Parallel Cylindrical Water Nanochannels in Nafion Fuel-cell Membranes, *Nat. Mater.* 7 (2008) 75-83.

[14] K.-D. Kreuer, G. Portale, A Critical Revision of the Nano-Morphology of Proton Conducting Ionomers and Polyelectrolytes for Fuel Cell Applications, *Adv. Funct. Mater.* 23 (2013) 5390-5397.

[15] A.-T. Kuo, W. Shinoda, S. Okazaki, Molecular Dynamics Study of the Morphology of Hydrated Perfluorosulfonic Acid Polymer Membranes, *J. Phys. Chem. C* 120 (2016) 25832-25842.

[16] A.-T. Kuo, K. Takeuchi, A. Tanaka, S. Urata, S. Okazaki, W. Shinoda, Exploring the effect of pendent side chain length on the structural and mechanical properties of hydrated perfluorosulfonic acid polymer membranes by molecular dynamics simulation, *Polymer* 146 (2018) 53-62.

[17] S. Yamamoto, S.-a. Hyodo, A Computer Simulation Study of the Mesoscopic Structure of the Polyelectrolyte Membrane Nafion, *Polym. J.* 35 (2003) 519-527.

[18] D. Wu, S.J. Paddison, J.A. Elliott, A comparative study of the hydrated morphologies of perfluorosulfonic acid fuel cell membranes with mesoscopic simulations, *Energy Environ. Sci.* 1 (2008) 284-293.

[19] D. Wu, S.J. Paddison, J.A. Elliott, Effect of Molecular Weight on Hydrated Morphologies of the Short-Side-Chain Perfluorosulfonic Acid Membrane, *Macromolecules* 42 (2009) 3358-3367.

- [20] D. Wu, S.J. Paddison, J.A. Elliott, S.J. Hamrock, Mesoscale Modeling of Hydrated Morphologies of 3M Perfluorosulfonic Acid-Based Fuel Cell Electrolytes, *Langmuir* 26 (2010) 14308-14315.
- [21] Y. Qi, Y.-H. Lai, Mesoscale modeling of the influence of morphology on the mechanical properties of proton exchange membranes, *Polymer* 52 (2011) 201-210.
- [22] K. Morohoshi, T. Hayashi, Modeling and Simulation for Fuel Cell Polymer Electrolyte Membrane, *Polymers* 5 (2013) 56.
- [23] A. Vishnyakov, A.V. Neimark, Self-Assembly in Nafion Membranes upon Hydration: Water Mobility and Adsorption Isotherms, *J. Phys. Chem. B* 118 (2014) 11353-11364.
- [24] R. Jorn, G.A. Voth, Mesoscale Simulation of Proton Transport in Proton Exchange Membranes, *J. Phys. Chem. C* 116 (2012) 10476-10489.
- [25] S. Liu, J. Savage, G.A. Voth, Mesoscale Study of Proton Transport in Proton Exchange Membranes: Role of Morphology, *J. Phys. Chem. C* 119 (2015) 1753-1762.
- [26] D.Y. Galperin, A.R. Khokhlov, Mesoscopic Morphology of Proton-Conducting Polyelectrolyte Membranes of Nafion® Type: A Self-Consistent Mean Field Simulation, *Macromol. Theor. Simul.* 15 (2006) 137-146.
- [27] J.T. Wescott, Y. Qi, L. Subramanian, T. Weston Capehart, Mesoscale simulation of morphology in hydrated perfluorosulfonic acid membranes, *J. Chem. Phys.* 124 (2006) 134702.
- [28] K. Malek, M. Eikerling, Q. Wang, Z. Liu, S. Otsuka, K. Akizuki, M. Abe, Nanophase segregation and water dynamics in hydrated Nafion: Molecular modeling and experimental validation, *J. Chem. Phys.* 129 (2008) 204702.
- [29] M. Ghelichi, K. Malek, M.H. Eikerling, Ionomer Self-Assembly in Dilute Solution Studied by Coarse-Grained Molecular Dynamics, *Macromolecules* 49 (2016) 1479-1489.
- [30] A.-T. Kuo, S. Okazaki, W. Shinoda, Transferable coarse-grained model for

perfluorosulfonic acid polymer membranes, *J. Chem. Phys.* 147 (2017) 094904.

[31] C. Peter, K. Kremer, Multiscale simulation of soft matter systems - from the atomistic to the coarse-grained level and back, *Soft Matter* 5 (2009) 4357-4366.

[32] T.A. Wassenaar, K. Pluhackova, R.A. Böckmann, S.J. Marrink, D.P. Tieleman, Going Backward: A Flexible Geometric Approach to Reverse Transformation from Coarse Grained to Atomistic Models, *J. Chem. Theory Comput.* 10 (2014) 676-690.

[33] M. Feig, P. Rotkiewicz, A. Kolinski, J. Skolnick, C.L. Brooks III, Accurate reconstruction of all-atom protein representations from side-chain-based low-resolution models, *Proteins* 41 (2000) 86-97.

[34] A.Y. Shih, P.L. Freddolino, S.G. Sligar, K. Schulten, Disassembly of Nanodiscs with Cholate, *Nano Lett.* 7 (2007) 1692-1696.

[35] P.J. Stansfeld, M.S.P. Sansom, From Coarse Grained to Atomistic: A Serial Multiscale Approach to Membrane Protein Simulations, *J. Chem. Theory Comput.* 7 (2011) 1157-1166.

[36] B. Hess, S. León, N. van der Vegt, K. Kremer, Long time atomistic polymer trajectories from coarse grained simulations: bisphenol-A polycarbonate, *Soft Matter* 2 (2006) 409-414.

[37] L. Thøgersen, B. Schiøtt, T. Vosegaard, N.C. Nielsen, E. Tajkhorshid, Peptide Aggregation and Pore Formation in a Lipid Bilayer: A Combined Coarse-Grained and All Atom Molecular Dynamics Study, *Biophys. J.* 95 (2008) 4337-4347.

[38] B. Ensing, S.O. Nielsen, Multiscale Molecular Dynamics and the Reverse Mapping Problem, in: T. Dumitrica (Ed.), Trends in Computational Nanomechanics: Transcending Length and Time Scales, Springer Netherlands, Dordrecht, 2010, pp. 25-59.

[39] A.J. Rzepiela, L.V. Schäfer, N. Goga, H.J. Risselada, A.H. De Vries, S.J. Marrink, Reconstruction of atomistic details from coarse-grained structures, *J. Comput. Chem.* 31(6) (2010) 1333-1343.

[40] P. Brocos, P. Mendoza-Espinosa, R. Castillo, J. Mas-Oliva, Á. Piñeiro, Multiscale

molecular dynamics simulations of micelles: coarse-grain for self-assembly and atomic resolution for finer details, *Soft Matter* 8 (2012) 9005-9014.

[41] S.C. Lovell, J.M. Word, J.S. Richardson, D.C. Richardson, The penultimate rotamer library, *Proteins* 40 (2000) 389-408.

[42] W. Shinoda, R. DeVane, M.L. Klein, Multi-property fitting and parameterization of a coarse grained model for aqueous surfactants, *Mol. Simul.* 33 (2007) 27-36.

[43] D.S. BIOVIA, Discovery Studio Modeling Environment, Release 2017, San Diego: Dassault Systèmes, 2016.

[44] C.M. MacDermaid, H.K. Kashyap, R.H. DeVane, W. Shinoda, J.B. Klauda, M.L. Klein, G. Fiorin, Molecular dynamics simulations of cholesterol-rich membranes using a coarse-grained force field for cyclic alkanes, *J. Chem. Phys.* 143 (2015) 243144.

[45] L. Martinez, R. Andrade, E.G. Birgin, J.M. Martinez, PACKMOL: A Package for Building Initial Configurations for Molecular Dynamics Simulations, *J. Comput. Chem.* 30 (2009) 2157-64.

[46] S. Plimpton, Fast Parallel Algorithms for Short-Range Molecular Dynamics, *J. Comput. Phys.* 117 (1995) 1-19.

[47] G.J. Martyna, M.L. Klein, M. Tuckerman, Nose-Hoover Chains: The Canonical Ensemble via Continuous Dynamics, *J. Chem. Phys.* 97 (1992) 2635-2643.

[48] M. Parrinello, A. Rahman, Polymorphic Transitions in Single Crystals: A New Molecular Dynamics Method, *J. Appl. Phys.* 52 (1981) 7182-7190.

[49] G.J. Martyna, D.J. Tobias, M.L. Klein, Constant Pressure Molecular Dynamics Algorithms, *J. Chem. Phys.* 101 (1994) 4177-4189.

[50] R.W. Hockney, J.W. Eastwood, Computer simulation using particles, CRC Press 1988.

[51] A.Z. Weber, J. Newman, Transport in Polymer-Electrolyte Membranes: II. Mathematical Model, *J. Electrochem. Soc.* 151 (2004) A311-A325.

- [52] S. Pronk, S. Páll, R. Schulz, P. Larsson, P. Bjelkmar, R. Apostolov, M.R. Shirts, J.C. Smith, P.M. Kasson, D. van der Spoel, B. Hess, E. Lindahl, GROMACS 4.5: A High-Throughput and Highly Parallel Open Source Molecular Simulation Toolkit, *Bioinformatics* 29 (2013) 845-854.
- [53] M.J. Abraham, T. Murtola, R. Schulz, S. Páll, J.C. Smith, B. Hess, E. Lindahl, GROMACS: High Performance Molecular Simulations Through Multi-Level Parallelism From Laptops to Supercomputers, *SoftwareX* 1–2 (2015) 19-25.
- [54] T. Mabuchi, T. Tokumasu, Effect of Bound State of Water on Hydronium Ion Mobility in Hydrated Nafion Using Molecular Dynamics Simulations, *J. Chem. Phys.* 141 (2014) 104904.
- [55] M. Levitt, M. Hirshberg, R. Sharon, K.E. Laidig, V. Daggett, Calibration and Testing of a Water Model for Simulation of the Molecular Dynamics of Proteins and Nucleic Acids in Solution, *J. Phys. Chem. B* 101 (1997) 5051-5061.
- [56] S.S. Jang, V. Molinero, T. Çağın, W.A. Goddard, Nanophase-Segregation and Transport in Nafion 117 from Molecular Dynamics Simulations: Effect of Monomeric Sequence, *J. Phys. Chem. B* 108 (2004) 3149-3157.
- [57] U. Essmann, L. Perera, M.L. Berkowitz, T. Darden, H. Lee, L.G. Pedersen, A smooth particle mesh Ewald method, *J. Chem. Phys.* 103 (1995) 8577-8593.
- [58] J. Liu, N. Suraweera, D.J. Keffer, S. Cui, S.J. Paddison, On the Relationship between Polymer Electrolyte Structure and Hydrated Morphology of Perfluorosulfonic Acid Membranes, *J. Phys. Chem. C* 114 (2010) 11279-11292.